Journal of Environmental Chemical Engineering 9 (2021) 106045

Contents lists available at ScienceDirect

Journal of Environmental Chemical Engineering

journal homepage: www.elsevier.com/locate/jece

Fabrication of GO–MnO_2 nanocomposite using hydrothermal process for cationic and anionic dyes adsorption: Kinetics, isotherm, and reusability

Monu Verma [a], Inderjeet Tyagi [b], Vinod Kumar [c,d], Simpy Goel [e], Dipti Vaya [e,*], Hyunook Kim [a,*]

[a] Water-Energy Nexus Laboratory, Department of Environmental Engineering, University of Seoul, Seoul 02504, Republic of Korea
[b] Centre of DNA taxonomy, Molecular Systematics Division, Zoological Survey of India, Kolkata 700053, India
[c] Department of Life Sciences, Graphic Era (Deemed to Be University), Dehradun, Uttarakhand 248002, India
[d] Peoples' Friendship University of Russia (RUDN University), Moscow 117198, Russian Federation
[e] Department of Chemistry, Amity School of Applied Sciences, Amity University, Haryana, 122413, India

ARTICLE INFO

Editor: Dr. GL Dotto

Keywords:
Hydrothermal method
Cationic and anionic dyes
Adsorption isotherm
Wastewater
Reusability

ABSTRACT

The presence of anionic and cationic dyes in wastewater has highlighted a great necessity to develop new and effective approaches for their simultaneous removal. Herein, graphene oxide-manganese dioxide (GO-MnO_2) nanocomposite was synthesized using a hydrothermal method to reduce pollution load of wastewater. In this stidy, synthesized material was utilized as adsorbent for the removal of cationic methylene blue (MB) and anionic methyl orange (MO) dyes from aqueous solution that act as model organic pollutants. The morphology, chemical structure, thermal stability, and other properties of the synthesized adsorbent were characterized using Field emmision scanning electron microscopy, Powder X-ray differaction, Raman spectroscopy, Fourier transform infrared spectra, Energy dispersive spectroscopy, Thermogravimetric analysis, and Brunauer-Emmett-Teller surface area techniques. The kinetics results showed the removal efficiency of 50.48% and 85.35% within the starting 5 min for both MO and MB, respectively, and fitted well to a pseudo-second-order kinetics model. The isotherms adsorption results fitted well to the Langmuir isotherm model, confirming the monolayer adsorption and give maximum adsorption capacities 149.253 and 178.253 mg/g for MO and MB, respectively. GO-MnO_2 showed a good reusability and gave > 90% removal efficiencies after seven continuous cycles. Lastly, the simultaneous adsorption performance of the adsorbent for both dyes ggave 100% removal efficiency. All these results give a direct visual impression of the fast kinetics efficiency and high adsorption capacity for real wastewater treatment application.

1. Introduction

Throughout the world, the discharging of excess organic dyes from different industries such as leather, cosmetics, textiles, paper etc. have the serious water polluted resources and caused a great damage to human health and aquatic system [1]. These different organic dyes are non-degradable, and create carcinogenic, breathing, vomiting, eye burns, diarrhea and nausea in human beings [2,3]. Therefore, removal of both cationic and anionic dyes from an aqueous system to avoid harmful effect on humans and environment is necessary and challenging task [4]. Till date, various physical, chemical, and biological processes including precipitation, coagulation, oxidation, membrane filtration, and adsorption methods for the successful elimination of various dyes from polluted water have been reported [5–9]. Among them, adsorption process is getting more attention due to lower cost, ecofriendly nature, and higher removal efficiency [10]. Unfortunately, this adsorption process suffered from poor selectivity and reusability, and low kinetics rate which restrict their further practical applications. Recently, many different types of adsorption reagents to remove different dyes from water have been used, which are expected to possess different advantages including cost effectiveness, high efficiency, low energy consumption, as well as good recyclable ability [11,12].

Exploration has been focused on finding inexpensive and environmentally friendly adsorbents for the removal of dyes or other various pollutants from water through adsorption. Graphene is a well-known 2-D carbon allotrope, consists of a atomic layer of graphite and sp^2 bonded carbon atoms organized in a hexagonal or honeycomb lattice which provide planarity [13]. It possesses high surface area (2630 m^2/g),

* Corresponding authors.
E-mail addresses: diptivaya08@gmail.com (D. Vaya), h_kim@uos.ac.kr (H. Kim).

https://doi.org/10.1016/j.jece.2021.106045
Received 20 May 2021; Received in revised form 1 July 2021; Accepted 10 July 2021
Available online 13 July 2021

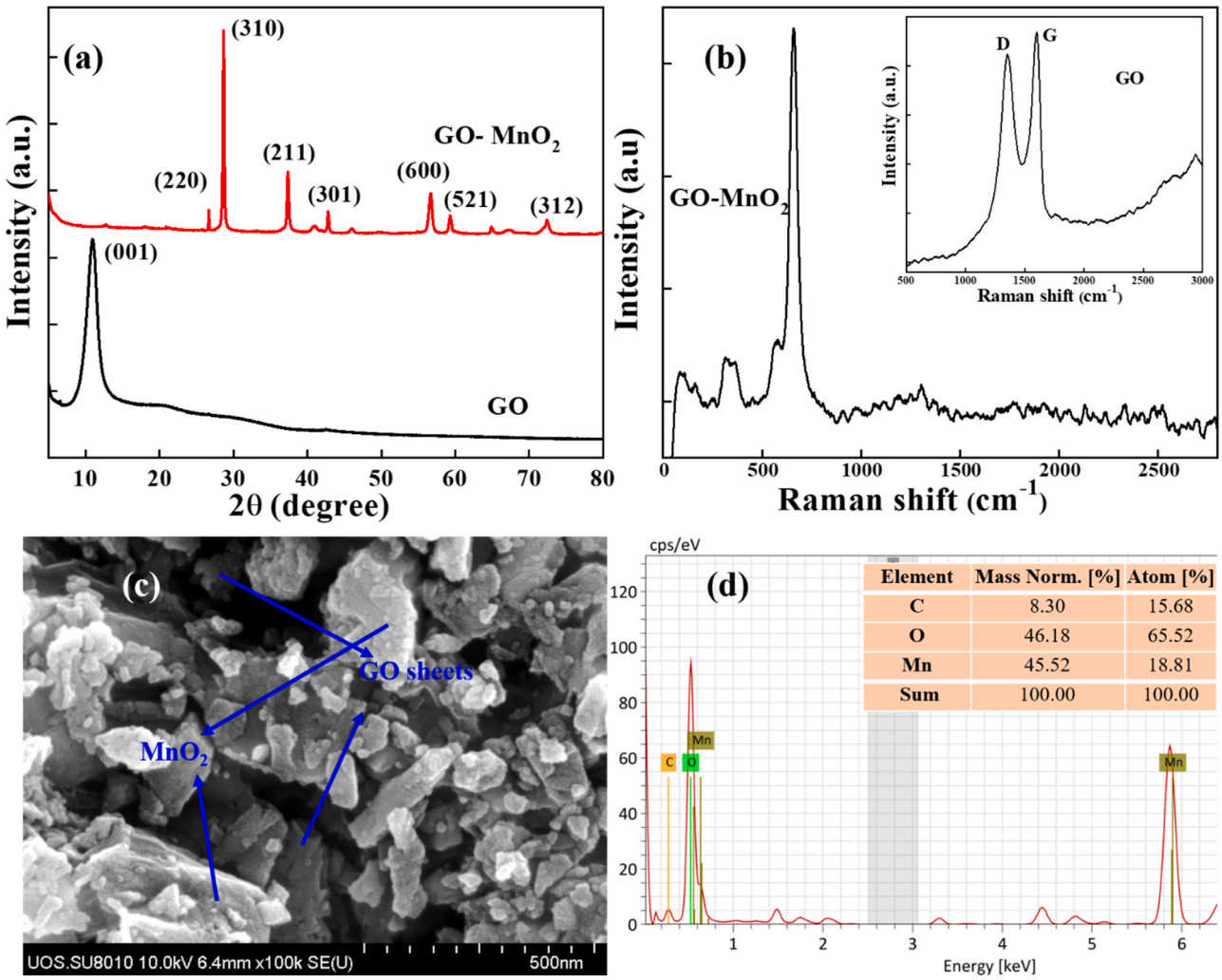

Fig. 1. (a) XRD patterns, (b) Raman spectrum (b) FE-SEM image, and (c) EDS spectrum and elemental composition (inset) of GO-MnO_2 nanocomposite.

excellent transparency, unmatched, conductivity, and good mechanical strength for different applications including wastewater treatment. However, the use of primitive graphene has proved challenging due to very low solubility [14], and easily agglomerated due to Vander Waals interactions [15].

Over the past few years, the research on composites of graphene oxide and reduced graphene oxide have attracted great attention because of their broad spectrum of applications in the various fields including removal of different types of pollutants from water [16–21]. Also, different metal oxides such as Fe_2O_3,TiO_2, ZnO_2, ZnO, Co_3O_4, GO-$CuFe_2O_4$ etc. have been utilized as promising materials due to relatively high surface area, low cost, and abundant availability in nature [22–25]. In them, nanosized manganese dioxide (MnO_2) has received a considerable interest due to its higher surface area and active sites, non-toxicity, lower cost, easy availability, and ecofriendly nature, which are necessary for a material to be a good adsorbent for environmental applications, especially in wastewater treatment [26–28]. Many researchers have reported the composites of MnO_2 as adsorbent to improve the adsorption properties and removal efficiency for different organic contaminants [29,30]. Graphene based metal and metal oxides nanocomposites were used for removal of different water pollutants from polluted water [31].

In this work, GO-MnO_2 nanocomposite was synthesized by simple one-pot hydrothermal process and characterized by using PXRD, FE-SEM, Raman, elemental mapping, EDS, FTIR, BET, and TGA techniques. Then, kinetics, isotherm and reusability analysis were investigated against typical cationic dye: Methylene blue (MB) and anionic dyes: Methyl orange (MO from aqueous solution.

2. Experimental work

2.1. Materials

All chemicals were used of analytical grade without any additional purification. Graphite powder (200 mesh), Sodium Nitrate ($NaNO_3$), Sulfuric Acid (H_2SO_4, 98% purity), Potassium Permanganate ($KMnO_4$), Hydrochloric acid (HCl, 37% purity), Hydrogen Peroxide (H_2O_2) were used of Thermo Fisher, India. Methylene blue (MB), and Methyl orange (MO) were procured from Sigma Aldrich, India.

2.2. Preparation of GO-MnO_2 nanocomposite

GO was synthesized using graphite flakes by modified Hummer's method as mentioned earlier by our group [32]. The nanocomposite of GO with MnO_2 was prepared according to one step hydrothermal process. Briefly, 500 mg $KMnO_4$ was dissolved in DI water and then 700 µL HCl was added slowly. Then 100 mL GO (50 mg) dispersed solution was added into the $KMnO_4$ solution and sonicated for 30 min to make it proper homogeneous solution. After that, this dispersed solution was shifted into a Teflon-lined stainless-steel autoclave and maintained 120°C temperature for 10 h, and then, allowed to cool at room temperature. After that, the product was washed several times with DI

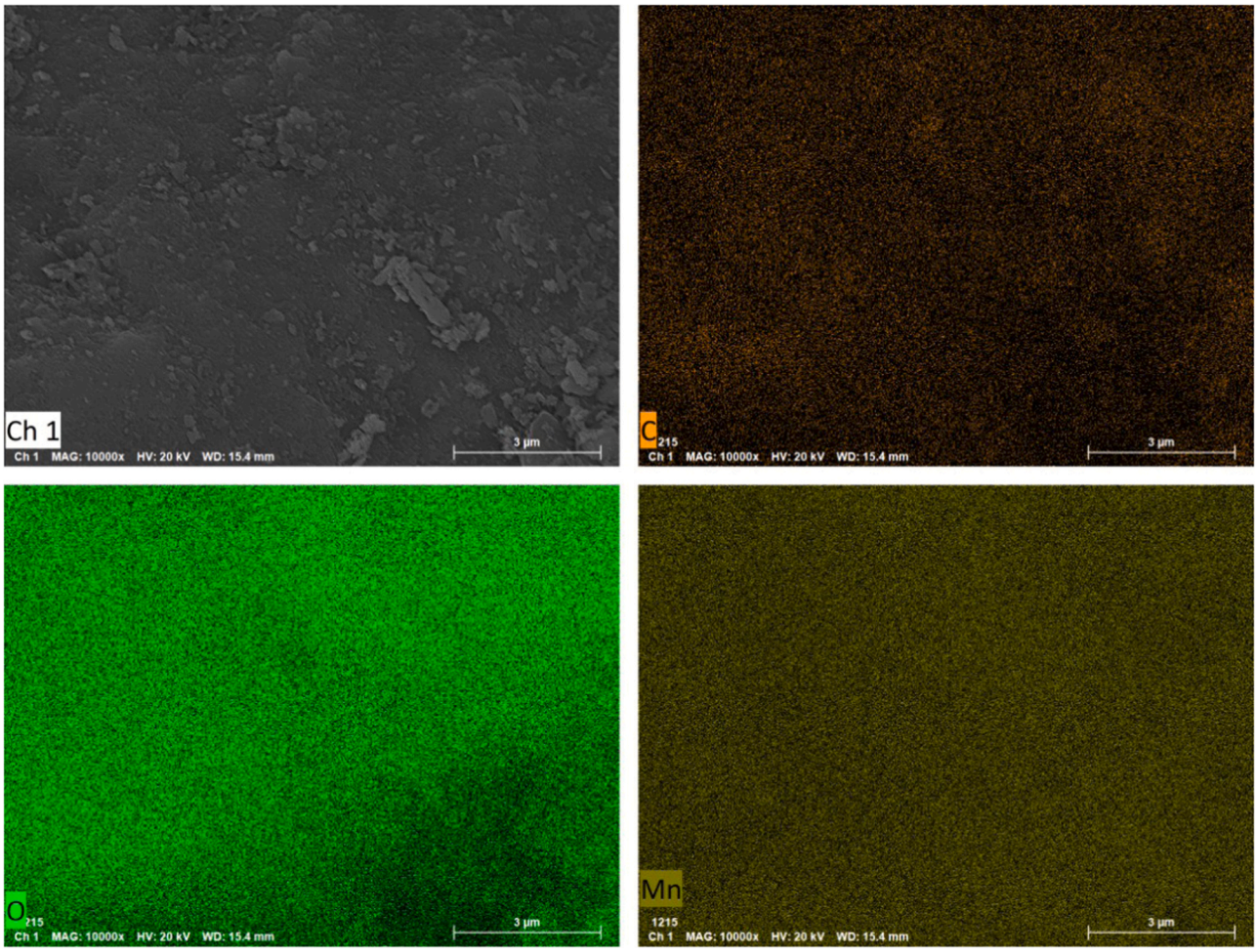

Fig. 2. Elemental mapping of synthesized GO-MnO_2 nanocomposite.

water, dried in vacuum oven at 50°C, and finally obtained the nanocomposite 1:5.50 (wt%/wt%) ratio of GO and MnO_2.

2.3. Batch adsorption experiments

The standard stock solutions 1000 mg/L concentrations of model pollutants MB and MO were prepared for further experiments. The pH of the solutions was maintained 4.3 and 10.5 for MO and MB dyes, respectively, by using 0.01 M NaOH and 0.01 M HCl solution for the experiments. The kinetics experiments were performed by using 50 mL volume of 150 mg/L initial concentration with 50 mg adsorbent at fixed interval 5, 10, 20, 30, 50, 80, 120, 180, and 300 min. The isotherm experiments were performed within concentration range (10–600 mg/L) using fix amount of adsorbent 50 mg for 24 h equilibrium time. The reusability experiments were performed up to seven cycles with initial 50 mg/L concentration. The experiments for simultaneous removal of both dyes from mixture were carried out at 7.12 pH with 100 mg/L initial concentration. For adsorption, the solution mixture was shaken vigorously at 25 °C at controlled incubator shaker with 150 rpm shaker speed, and then the samples were separated using 0.45 µm syringe filter. The initial and final concentrations of the MB and MO dyes were analyzed using UV-Vis spectrometer at a wavelength of 663 and 464 nm, respectively. The removal efficiency (%) and adsorption capacity (Q_e) were calculated according to Eqs. (1) and (2):

$$\% \text{ Removal} = \frac{(C_o - C_e)}{C_o} \times 100 \quad (1)$$

$$Q_e = (C_o - C_e) \times \frac{V}{W} \quad (2)$$

where, Q_e (mg/g) is the adsorption capacity of the adsorbent at equilibrium; C_o and C_e (mg/L) are the initial and equilibrium concentrations of dyes, respectively; V (mL) is the volume of the solution and W (g) is the weight of adsorbent. The point of zero charge (pH_{zpc}) of the GO-MnO_2 nanocomposite was examined using pH drift method which was found to be 4.7. This pH_{ZPC} is closer to earlier reported value [33].

2.4. Characterizations

The crystalline phase, structure, and purity of the synthesized GO and GO-MnO_2 nanocomposite were analyzed using high resolution powder X-ray diffraction (PXRD), Rigaku (Smartlab), Japan, using monochromatic Cu K_α radiation (Kα = 1.541 Å) with scan speed 2°/min, step size 0.02 in the range of 5–80°. Raman spectra were measured on Raman microscopy (XploRA PLUS, Horiba company, Japan) at excitation wavelength 785 nm. The surface functional groups of the synthesized adsorbent were examined using Fourier transform infrared spectroscopy (FT–IR), Nexus 670, Thermo Electron Corporation, United States in the range of 400–3800 cm^{-1}. The surface morphology and microstructure information were examined by Field emission scanning electron microscopy (FE-SEM), SU-8010, Hitachi, Japan) at working voltage 10.0 kV voltage. The elemental mapping and compositional analysis were investigated with the Energy dispersive X-ray spectroscopy (EDS) attached with FE-SEM. The values of specific surface area and porosity of GO-MnO_2 were measured by BET

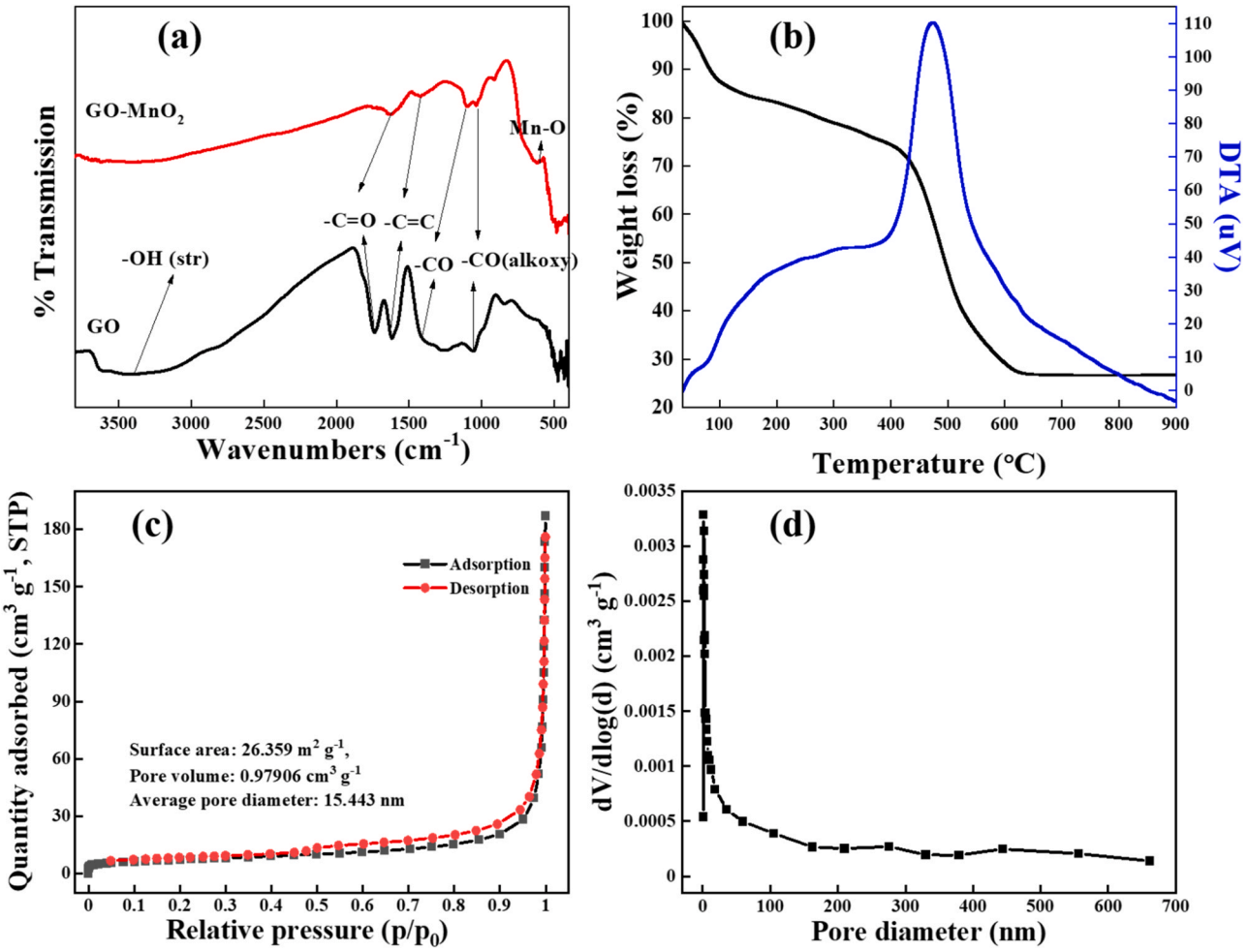

Fig. 3. (a) FT-IR spectrum of GO and GO-MnO_2 nanocomposite, (b) combined graph of TGA and DTA, (d) N_2 adsorption-desorption isotherm, and (d) pore size distribution of GO-MnO_2 nanocomposite.

(Brunauer–Emmett–Teller) and BJH (Barrett-Joyner-Halenda) methods, respectively on BelsorpX mini, MicrotracBEL Corp. (Japan) at 77.35 K using N_2 adsorption-desorption test. The thermal stability was investigated on Thermogravimetric analyzer (TGA), EXSTAR 6300. The samples were heated 10 °C/min heating rate under N_2 atmosphere in the range of 35–900°C. The initial and final dyes concentration was examined by measuring the absorbance on UV-Vis spectrophotometer, UV-2600 model, Shimadzu Company.

3. Results and discussions

3.1. Characterizations

The powder XRD patterns of the synthesized GO and GO-MnO_2 nanocomposite are represented in Fig. 1(a). GO exhibits a sharp peak at 10.5° corresponding to the (001) reflection, which confirms the successful formation of GO via oxidation of graphite. The prepared GO-MnO_2 nanocomposite showed the different diffraction peaks situated at $2\theta = 26.4°$, 28.8°, 37.5°, 42.78°, 56.74°, and 60.3° and 72.55°which are corresponding to diffraction plans (220), (310), (211), (301), (600), (521), and (312) of tetragonal phase of MnO_2 according to JCPDS file no. 00–044–0141 (space group:I4/m; $a = b = 9.7847$,$c = 2.8630$; $\alpha = \beta = \gamma = 90°$). In the PXRD pattern of GO-MnO_2 nanocomposite, the peak (001) of GO nearly disappeared, which may be due to the diffraction signals of oxygen-containing groups of MnO_2. Earlier, it was also mentioned that diffraction peaks become reduced or even vanish due to increasing or decreasing the content of GO. Also, another reason behind the loss of GO peaks may be the exfoliation of the regular lamellar structure of GO sheets [34].

The crystallite size of GO-MnO_2 was calculated by Debye- Scherrer's equation which is given as:

$$D = k\lambda/\beta \cos\theta \quad (3)$$

The crystallite size of GO-MnO_2 nanocomposite for the major diffraction peak attributed to (310) was found to be about 31.72 nm. In the PXRD patterns, no other peak of any impurity or other raw materials were observed in the synthesized GO and GO-MnO_2 nanocomposite, confirming the formation of high purity materials. The Raman spectrums of the synthesized GO and GO-MnO_2 nanocomposite are given in Fig. 1(b). GO shows two major peaks at 1590 and 1350 cm^{-1}, indicating the G band and D band of carbon based compound [35]. The intensity ratio of the G band and D band ($R=I_G/I_D$) represents degree of graphitization, and a higher ratio indicates good quality of the graphitization. In the current GO synthesis, this calculated ratio is 1.013, indicating that sample shows high graphitization in turn better quality and high conductivity. GO-MnO_2 nanocomposite shows another sharp peak which appears at 662 cm^{-1} represents Mn–O stretching vibration, and D and G band nearly disappear due to smaller concentration of used GO [36]. This Raman data strongly supported to the XRD results. FE-SEM image of GO-MnO_2 nanocomposite is shown in Fig. 1(c). The particles of MnO_2 are uniformly distributed over the exfoliated and aligned sheets of GO which are forming a 2D network with little bit aggregation. The MnO_2 nanoparticles seem to be sharp, a crystal-like structure having small rods

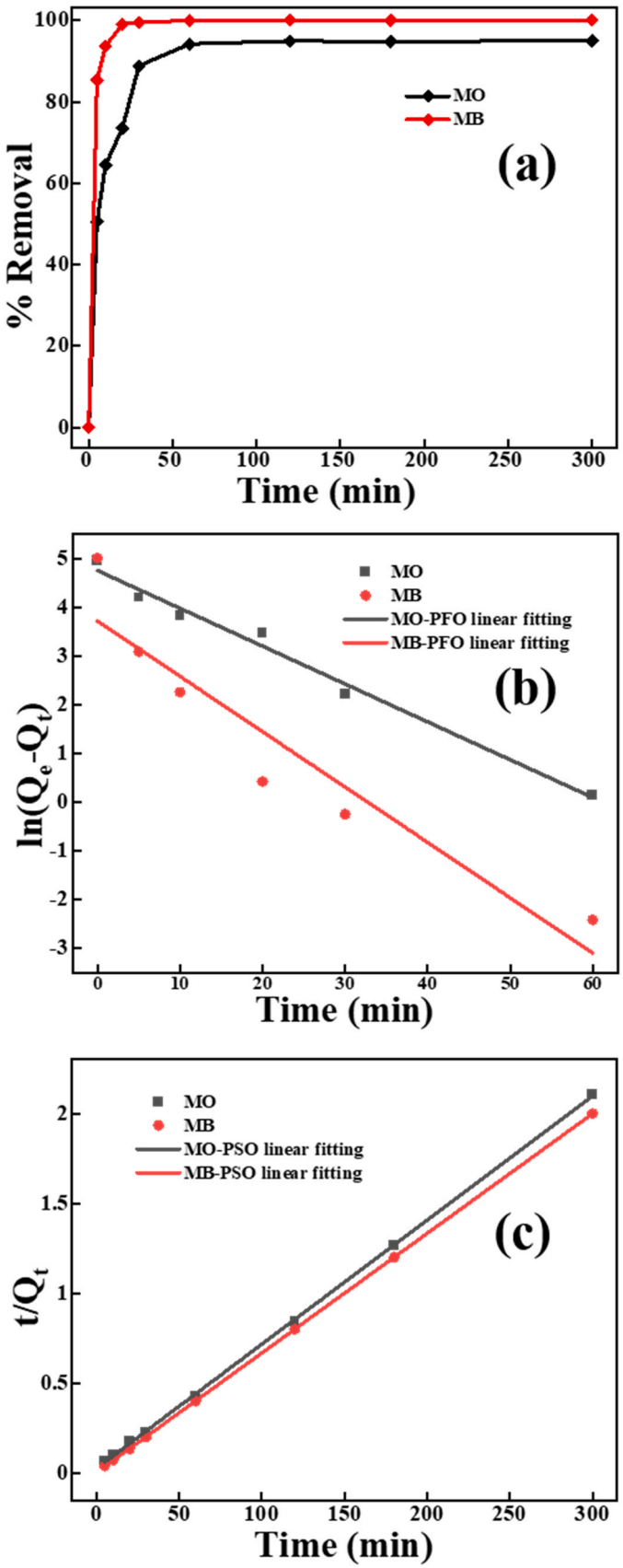

Fig. 4. (a) Effect of contact time, and linear fitting kinetics model (b) PFO, and (c) PSO for MO and MB dyes adsorption towards GO-MnO_2 adsorbent (dose = 50 mg/50 mL solution, pH = 4.3 and 10.5 for MO and MB dyes respectively).

and little bit of spherical shape. These sharp structures and highly focused images show the highly crystalline nature of MnO_2 in GO-MnO_2 nanocomposite. The EDS spectrum of the synthesized GO-MnO_2 is presented in Fig. 1(d) to examine the purity and elemental composition. The spectrum shows the presence of only C (at. 15.68%), O (at. 65.52%), and Mn (at. 18.81%) elements, which are highly pure as according to our expectations (Table in inset of Fig. 1(d)). Furthermore, the elemental mapping of GO-MnO_2 nanocomposite is shown in Fig. 2, which clearly indicating the uniform distribution of C, O, and Mn elements throughout the surface. FTIR spectrum of synthesized GO and nanocomposite are shown in Fig. 3(a). In GO, peaks observed at 3404, 1733, 1622, 1403 and 1116 cm^{-1} which are corresponding to the stretching vibration of hydroxyl groups, carbonyl group of carboxylic acid, olefine group, ether, and alkoxy C–O groups, respectively [37]. These peaks indicated that graphite was successfully converted into GO. All peaks of GO reflected in FTIR of GO-MnO_2 nanocomposite, only peaks intensity was reduced due to binding of GO with MnO_2 which confirmed the nanocomposite formation. Along with the one additional peak showed at 511 cm^{-1} in nanocomposite could be assigned to Mn–O vibration of the GO-MnO_2 nanocomposite [38]. The TGA data exhibits three weight loss stages as represented in Fig. 3(b). The first stage shows the decline weight of 13.5% up to 110 °C due to loss of adsorbed moisture content. The second step indicates weight loss of 12.5% in the range 110–390 °C due to removal of the oxygen-bearing functional groups. The third stage indicates the loss of 47% in the range of 300–600 °C which indicates the thermal decomposition of GO and the evolution of oxygen by conversion of MnO_2 into Mn_2O_3 (~ 470 °C) [39]. DTA graph displays only one major peak between 410 °C and 550 °C probably due to the transformation of Mn (IV) to Mn(III). N_2 adsorption-desorption of the synthesized GO-MnO_2 is shown in Fig. 3(c). The isotherm is typical IV, with hysteresis loops type H3, indicating the mesoporous structure with a relative pressure between 0 and 1. The BET specific surface area, cumulative pore volume and average pore diameter were measured to be 26.359 m^2/g, 0.97906 cm^3/g, and 15.443 nm, respectively. Pore size distribution in the GO-MnO_2 adsorbent is given in Fig. 3(d), indicating broad pore size distribution with a maximum value at 2 nm.

3.2. *Effect of contact time and kinetics*

The contact time effect is an important parameter for the analysis of equilibrium between adsorbate and adsorbent. Fig. 4(a) indicates the effect of contact time on dyes removal which shows 50.48% and 85.35% removal efficiency in starting 5 min and attends equilibrium in 60 and 20 min with the removal of 94.17%, and 98.98% for MO and MB dyes, respectively. The fast adsorption for MB was observed in comparison to MO dye due to more interaction between existing opposite charges on GO-MnO_2 nanocomposite and MB dyes than GO-MnO_2 nanocomposite with MO. Also, the faster adsorption in the earlier time was attributed to the sufficient surface area and availability of reactive sites on the adsorbent which became saturated to attend equilibrium.

Pseudo-first-order (PFO) and Pseudo-second-order (PSO) kinetic models were measured to investigate the adsorption mechanism of dyes onto the surface of GO-MnO_2 nanocomposite. The PFO kinetic model describes that the rate of change in solute adsorption is directly proportional to the change observed over time between saturated and the adsorptive solid concentration, while PSO kinetic model assumes that the rate of adsorption is measured through interaction between the adsorbate and adsorbent. The PFO and PSO kinetics model in the linear form are given below Eqs. 4 and 5, respectively [40]:

$$\ln(Q_e - Q_t) = \ln Q_e - k_1 t \quad (4)$$

$$\frac{t}{Q_t} = \frac{1}{k_2 Q_e^2} + \frac{t}{Q_e} \quad (5)$$

where, Q_e and Q_t are the amounts of dyes adsorbed (mg/g) on the surface of adsorbent at equilibrium and at a given time t (min), respectively,

Table 1
Adsorption kinetic parameters of MB and MO dyes onto GO-MnO_2 adsorbent.

Dye	Pseudo first order			Pseudo second order		
	R^2	k_1 (min^{-1})	Q_e (mg/g)	R^2	k_2 (g/mg·min)	Q_e (mg/g)
MO	0.975	0.0776	116.16	0.999	0.0018	144.927
MB	0.896	0.113	67.96	0.999	0.0156	150.375

k_1 (per min) and k_2 (g/mg. min) are the rate constant for PFO and PSO kinetics, respectively. The linear plot between $\ln(Q_e - Q_t)$ versus t and t/Q_t versus t for PFO and PSO linear fitting are presented in Fig. 4(b) and (c), respectively, and kinetics parameters are showed in Table 1. The value of correlation coefficient (R^2) for PSO kinetic model had excellent fitting ($R^2 > 0.99$) for both MO and MB dyes in comparison PFO, which clearly depicts that the PSO rate adsorption process is predominant through chemisorption rate determining step. Also, a higher value of rate constant (k) for MB confirms a faster adsorption rate towards cationic dyes than anionic dyes.

3.3. Effect of initial concentration and adsorption isotherm

The effect of initial dyes concentration on the removal efficiency was studied in the range of 10–600 mg/L concentrations and the removal efficiency data is plotted in Fig. 5(a). Fig. clearly shows that as the concentration was increased from 10 mg/L to 600 mg/L, the removal efficiencies decreased from 100% to 29.63% and 24.88% for MB and MO, respectively. The adsorption capacities were enhanced from 10 to 177.83 mg/g and 10–149.28 mg/g for MB and MO dyes, respectively. This might be due to an increase in the initial dye concentration cause the adsorption sites on the GO-MnO_2 adsorbent surface to be saturated, which leads to a decrease in the removal efficiency. Opposite of this trend, an increase in dye concentration causes the adsorption capacity of the adsorbent to increase.

Two famous isotherm models Langmuir and Freundlich were used to investigate the phenomena that occurred at the surface of the nanocomposite during the adsorption process. Langmuir isotherm model [41] describes monolayer surface and homogeneous adsorption process. The linearized form can be expressed according to Eq. (6):

$$C_e/Q_e = C_e/Q_m + 1/K_L Q_m \quad (6)$$

Freundlich isotherm model [42] describes heterogeneous sites with a non-uniform distribution. The linearized equation can be written as Eq. (7):

$$\ln Q_e = \ln K_F + 1/n(\ln C_e) \quad (7)$$

where C_e (mg/L) is the concentration of dyes in equilibrium solution, and K_L (L/g) is the Langmuir adsorption constant. Q_e and Q_m(mg/g) are the amounts of dyes (mg/L) adsorbed on adsorbent at equilibrium and maximum adsorption capacity of GO-MnO_2 nanocomposite, respectively. K_F ($mg^{1-1/n}\ L^{1/n}/g$) and n are Freundlich adsorption equilibrium constant and adsorption intensity constants for the Freundlich adsorption isotherm, respectively. The value of 1/n shows different types of isotherms: $1/n = 0$ means the adsorption is either irreversible, $0 < 1/n < 1$ means favorable adsorption, and$1/n > 1$ means the contrary [43]. The linear fitting plots for Langmuir and Freundlich isotherm models are shown in Fig. 5(b) and (c), and their corresponding calculated parameters are listed in Table 2. Table 2 indicates the better correlation coefficient ($R^2 \geq 0.99$) value and closer calculated $Q_{m,cal}$ values with experimental $Q_{m,exp}$ values for Langmuir model than the Freundlich model, which is a criterion for the fitting degree for the system. This better fitting indicating monolayer adsorption of both MB and MO dyes onto GO-MnO_2 nanocomposite which are occupied on the homogeneous surface of the adsorbent. The value of 1/n for both dyes exists between $0 < 1/n < 1$, confirming the favorable adsorption process. The

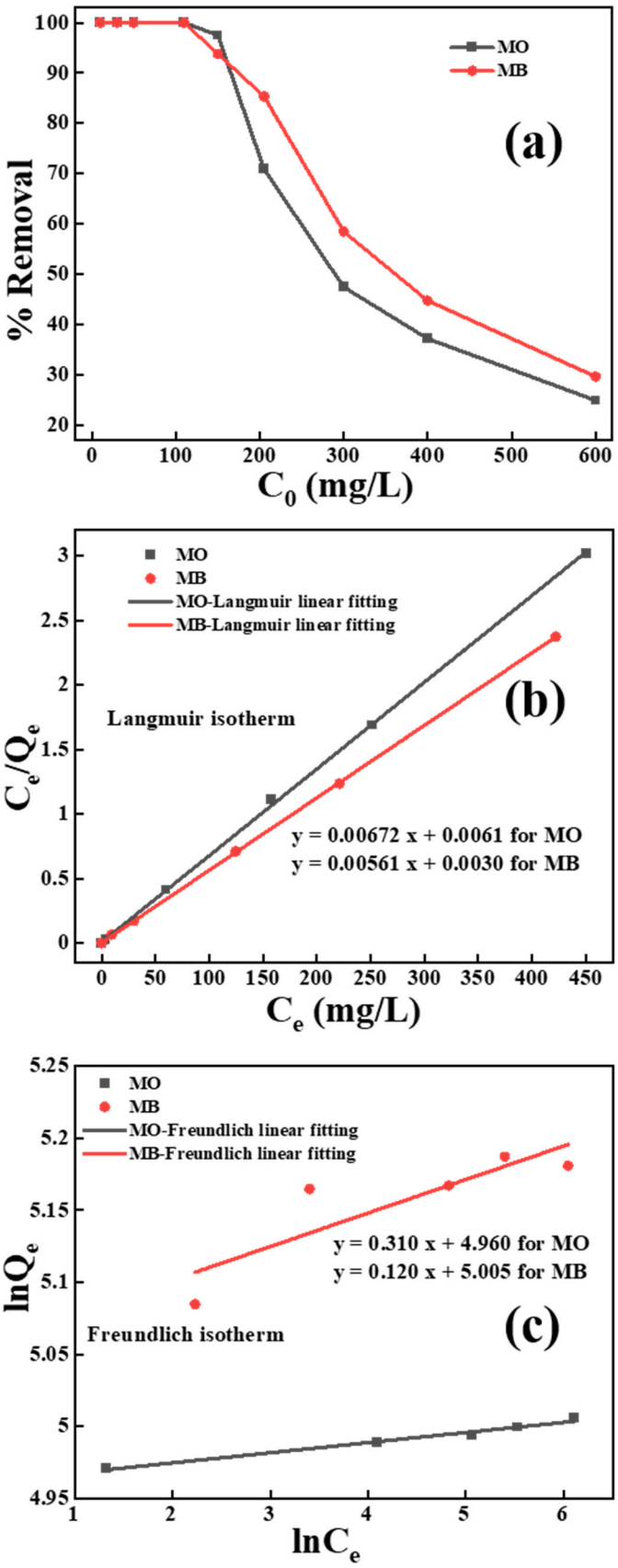

Fig. 5. (a) Effect of initial concentration, and linear fitting data for (b) Langmuir, and (c) Freundlich isotherm for MO and MB dyes adsorption onto GO-MnO_2 adsorbent.

Table 2
Isotherms parameters for MB and MO dyes.

Dye		Langmuir			Freundlich		
	$Q_{m,\ exp}$	R^2	K_L	$Q_{m,\ cal.}$ (mg/g)	R^2	1/n	K_F
MO	149.289	0.999	1.101	149.253	0.980	0.007	142. 593
MB	177.836	0.999	1.827	178.253	0.966	0.023	149.157

Table 3
Comparison of adsorption capacity with various adsorbent materials for MB and MO dyes.

Adsorbent	Pollutant	Kinetic order and rate constant (g/mg.min)	Isotherm model; Adsorption capacity (mg/g)	Refs.
KOH modified Metroxylon spp	MB	Pseudo second order, 4.28×10^{-8}	Langmuir; 212.8	[46]
Blast furnace slag acid-alkali precipitate (BFSAP)	MO	Pseudo second order, 1.429×10^{-6}	Langmuir; 167	[47]
Acetic acid and L-arginine impregnated adsorbents Populous leaves	MO	Pseudo first order,59×10^{-3}	Langmuir; 90.44	[48]
FeOOH/ carbonized bacterial cellulose nanocomposite	MO	–	Langmuir and Frundlich; 107.68	[49]
Modified activated carbon	MB	Pseudo second order, 1.9×10^{-4}	Langmuir; 47.62	[50]
Graphene oxide nanocomposite	MB	Pseudo first order, 5.6×10^{-3}	–	[51]
Cellulose based nanocomposite	MB	Pseudo second order 4.4×10^{-3}	Frundlich;41.36	[52]
GO-MnO_2 Nanocomposite	MB	Pseudo second order, 15.6×10^{-3},	Langmuir 178	This study
	MO	1.8×10^{-3}	149	

calculated Q_m values from the Langmuir model were 178.23 and 149.253 mg/g for MB and MO dyes, respectively.

A comparison of adsorption capacities of different adsorbents with current synthesized GO-MnO_2 nanocomposite adsorbent towards MB and MO dyes has been listed in Table 3. Table clearly shows good adsorption capacity of GO-MnO_2 nanocomposite for MB and MO dyes adsorption that of other presented adsorbents. Also, synthesized GO-MnO_2 nanocomposite needed a shorter time for equilibrium state compared to some other reported adsorbents.

3.4. Regeneration and reusability of adsorbent

Recyclability and reusability are other important parameters of any adsorbent for the practical application purpose. The desorption was carried out using 0.1 N HCl and 0.1 N NaOH for MB and MO dyes, respectively [44,45]. The recyclability was carried out using 50 mg GO-MnO_2 nanocomposite adsorbent with 50 mL solution of 50 mg/L initial dyes concentration at solution pH 4.3 and 10.5 for MO and MB dyes, respectively. The performance for seven successive cycles is shown in Fig. 6(a). The results indicate a very slight decrement in the adsorptive removal efficiency after three cycles and it was more than 90% after continuing seven cycles. Thus, for the practical purpose, the synthesized GO-MnO_2 nanocomposite could be a good adsorbent for the wastewater treatment containing cationic and anionic dyes.

3.5. Simultaneous removal of MB and MO dyes

The removal efficiency was also investigated by taking individual 100 mg/L initial concentrations and a mixture of both dyes using pH 4.3, 10.5, and 7.12 for MO, MB, and mixtures, and almost 100% removal in both dyes was observed. These experiments were carried using syringe and the image of the dyes before and after adsorption are represented in

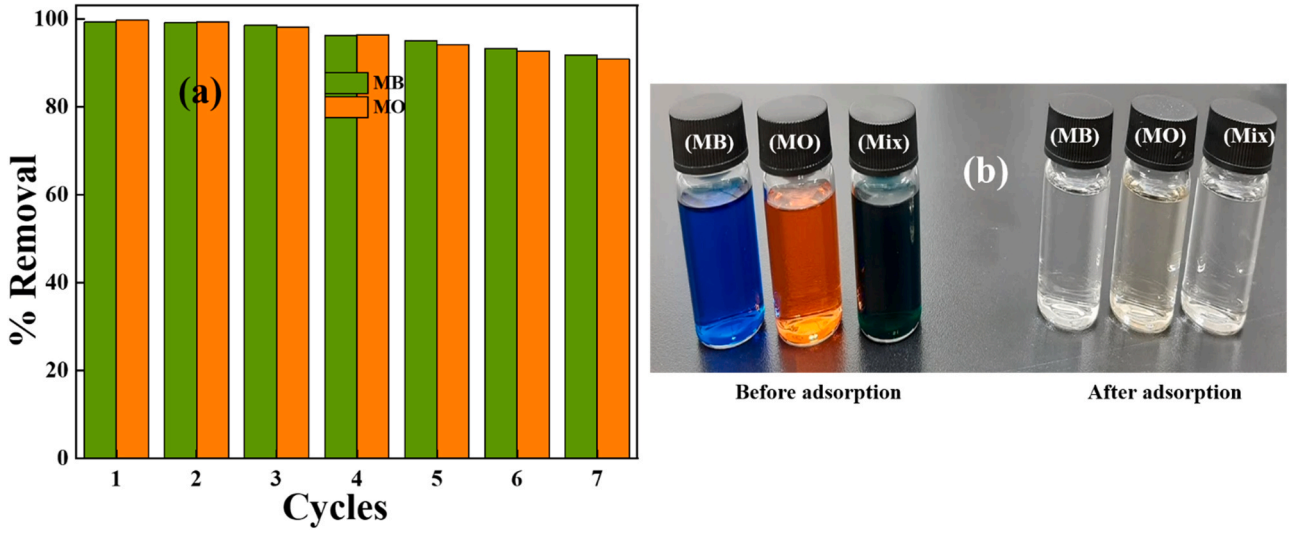

Fig. 6. (a) Reusability performance of GO-MnO_2 nanocomposite by seven cycles of adsorption/desorption. Initial concentration: 50 mg/L, dose: 50 mg, pH: 4.3 and 10.5 for MOand MB dyes, respectively (b) Image of individual and mixture of dyes before and after the adsorption. Initial concentrations: 100 mg/L, pH: 4.3, 10.5 and 7.12 for MO, MB and mixture, respectively.

Fig. 6(b) which clearly indicating the fast removal efficiency of both dyes for practical purposes.

4. Conclusions

In summary, GO-MnO_2 nanocomposite was synthesized using hydrothermal process and used for the removal of cationic MB and anionic MO dyes from the aqueous solution. The different characterizations PXRD, Raman, elemental mapping, and FT-IR confirm the formation of high purity adsorbent with uniform elemental distribution. GO-MnO_2 nanocomposite showed sufficient potential in the removal of MB and MO dyes from the aqueous solution. The rapid removal 50.48% of MO, and 85.35% of MB occurred in starting 5 min, and further, about 94.17% of MO and 100% of MB dyes were adsorbed within 60 min. Kinetics results followed to PSO kinetics model. The isotherm model fitted well with Langmuir isotherm model and showed maximum adsorption capacities 149.253 and 178.253 mg/g for MO and MB dyes, respectively. The regenerated GO-MnO_2 adsorbent showed more than 90% removal efficiency after seven continuous cycles. The simultaneous removal results of both dyes at lower and higher concentrations give 100% removal efficiency. From these results, it can be assumed that the synthesized adsorbent can be used for column packing in column fabrication to purify the water by filtration. By considering the low cost and higher adsorption potential, GO-MnO_2 nanocomposite will be becoming a promising candidate for simultaneous removal of cationic and anionic dyes from polluted water for water purification.

CRediT authorship contribution statement

On the approval of all authors, contribution of each author in the manuscript is as follows: **Monu Verma**: Conceptualization; Data curation; Investigation; Methodology. **Inderjeet Tyagi**: Formal analysis. **Vinod Kumar:** Investigation; Methodology. **Simpy Goel**- Methodology; Original draft. **Dipti Vaya**: Supervision, Investigation and Review. **Hyunook Kim:** Supervision, Investigation and Review.

Declaration of Competing Interest

The authors declare that they have no known competing financial interests or personal relationships that could have appeared to influence the work reported in this paper.

Acknowledgments

Monu Verma would like to thanks to National Research Foundation of Korea (NRF) for providing funding by the Ministry of Science and ICT by the Brain Pool Program (2019H1D3A1A01102657). This paper has been also supported by the RUDN University Strategic Academic Leadership Program. Dipti Vaya would like to acknowledge the support provided under the DST-FIST Grant No. SR/FST/PS-I/2019/68 of Govt. of India.

References

[1] L. Shen, Z. Jin, W. Xu, X. Jiang, Y.X. Shen, Y. Wang, Y. Lu, Enhanced treatment of anionic and cationic dyes in wastewater through live bacteria encapsulation using graphene hydrogel, Ind. Eng. Chem. Res. 58 (2019) 7817–7824, https://doi.org/10.1021/acs.iecr.9b01950.

[2] M. Ismail, K. Akhtar, M.I. Khan, T. Kamal, M.A. Khan, A.M. Asiri, Pollution, toxicity and carcinogenicity of organic dyes and their catalytic bio-remediation pollution, toxicity and carcinogenicity of organic dyes and their catalytic bio-remediation, Curr. Pharm. Des. 25 (2019) 3653–3671, https://doi.org/10.2174/1381612825666191021142026.

[3] S. Jiang, T. Yu, R. Xia, X. Wang, M. Gao, Realization of super high adsorption capability of 2D δ-MnO_2/GO through intra-particle diffusion, Mater. Chem. Phys. 232 (2019) 374–381, https://doi.org/10.1016/j.matchemphys.2019.05.004.

[4] M. Daud, A. Hai, F. Banat, M.B. Wazir, M. Habib, G. Bharath, M.A. Al-Harthi, A review on the recent advances, challenges and future aspect of layered double hydroxides (LDH)– Containing hybrids as promising adsorbents for dyes removal, J. Mol. Liq. 288 (2019), 110989, https://doi.org/10.1016/j.molliq.2019.110989.

[5] F.E. Aboelfetoh, E.A. Aboubaraka, M.E.-Z. Ebeid, Binary coagulation system (graphene oxide/chitosan) for polluted surface water treatment, J. Environ. Manag. 288 (2021), 112481, https://doi.org/10.1016/j.jenvman.2021.112481.

[6] A. Saravanana, P.S. Kumar, S. Jeevanantham, S. Karishma, B. Tajsabreen, P. R. Yaashika, B. Reshma, Effective water/wastewater treatment methodologies for toxic pollutants removal: processes and applications towards sustainable development, Chemosphere 280 (2021), 130595, https://doi.org/10.1016/j.chemosphere.2021.130595.

[7] T. Chen, B. Li, W. Huang, C. Lin, G. Li, H. Ren, Y. Wu, S. Chen, W. Zhang, H. Ma, Highly crystalline ionic covalent organic framework membrane for nanofiltration and charge-controlled organic pollutants removal, Sep. Purif. Technol. 256 (2021) 117787–117796, https://doi.org/10.1016/j.seppur.2020.117787.

[8] M. Verma, K.P. Singh, A. Kumar, Reactive magnetron sputtering based synthesis of WO_3 nanoparticles and their use for the photocatalytic degradation of dyes, Solid State Sci. 99 (2020), 105847, https://doi.org/10.1016/j.solidstatesciences.2019.02.008.

[9] Q. Yang, Y. Ma, F. Chen, F. Yao, J. Sun, S. Wang, K. Yi, L. Hou, X. Li, D. Wang, Recent advances in photo-activated sulfate radical-advanced oxidation process (SR-AOP) for refractory organic pollutants removal in water, Chem. Eng. J. 378 (2019), 122149, https://doi.org/10.1016/j.cej.2019.122149.

[10] S. De Gisi, G. Lofrano, M. Grassi, M. Notarnicola, Characteristics and adsorption capacities of low-cost sorbents for wastewater treatment: a review, Sustain. Mater. Technol. 9 (2016) 10–40, https://doi.org/10.1016/j.susmat.2016.06.002.

[11] L. Li, R. Chen, T. Hu, Y. Li, Q. Wang, C. He, Novel magnetic pillar[5]arene polymer as adsorbent for rapid removal of organic pollutants in water or air, Microchem. J. 153 (2020) 1–7, https://doi.org/10.1016/j.microc.2019.104524.

[12] P. Sirajudheena, K. Perumal, R. Krishnapillai, P. Nisheetha, S. Meenakshi, Magnetic carbon-biomass from the seeds of Moringa oleifera@$MnFe_2O_4$ composite as an effective and recyclable adsorbent for the removal of organic pollutants from water, J. Mol. Liq. 327 (2021), 114829, https://doi.org/10.1016/j.molliq.2020.114829.

[13] C.N.R. Rao, A.K. Sood, K.S. Subrahmanyam, A. Govindaraj, Graphene: the new two-dimensional nanomaterial, Angew. Chem. Int. Ed. 48 (2009) 7752–7777, https://doi.org/10.1002/anie.200901678.

[14] S. Niyogi, E. Bekyarova, M.E. Itkis, J.L. McWilliams, M.A. Hamon, R.C. Haddon, Solution properties of graphite and graphene, J. Am. Chem. Soc. 128 (2006) 7720–7721.

[15] T. Kuilla, S. Bhadra, D. Yao, N.H. Kim, S. Bose, J.H. Lee, Recent advances in graphene based polymer composites, Prog. Polym. Sci. 35 (2010) 1350–1375.

[16] A.T. Smith, A.M. LaChance, S. Zeng, B. Liu, L. Sun, Synthesis, properties, and applications of graphene oxide/reduced graphene oxide and their nanocomposites, Nano Mater. Sci. 1 (2019) 31–47, https://doi.org/10.1016/j.nanoms.2019.02.004.

[17] I.A. Mkhalid, A. Shawky, Visible light-active CdSe/rGO heterojunction photocatalyst for improved oxidative desulfurization of thiophene, Ceram. Int. 46 (2020) 20769–20776, https://doi.org/10.1016/j.ceramint.2020.05.033.

[18] M. Alhaddad, A. Shawky, Superior photooxidative desulfurization of thiophene by reduced graphene oxide-supported MoS_2 nanoflakes under visible light, Fuel Process. Technol. 205 (2020), 106453, https://doi.org/10.1016/j.fuproc.2020.106453.

[19] S.I. El-hout, S.M. El-sheikh, A. Gaber, A. Shawky, A.I. Ahmed, Highly efficient sunlight-driven photocatalytic degradation of malachite green dye over reduced graphene oxide-supported CuS nanoparticles, J. Alloys Compd. 849 (2020), 156573, https://doi.org/10.1016/j.jallcom.2020.156573.

[20] M. Alhaddad, A. Shawky, CuS assembled rGO heterojunctions for superior photooxidation of atrazine under visible light, J. Mol. Liq. 318 (2020), 114377, https://doi.org/10.1016/j.molliq.2020.114377.

[21] M. Alhaddad, A. Shawky, Z.I. Zaki, Reduced graphene oxide-supported $PbTiO_3$ nanospheres: improved ceramic photocatalyst toward enriched photooxidation of thiophene by visible light, Mol. Catal. 499 (2021), 111301, https://doi.org/10.1016/j.mcat.2020.111301.

[22] R. Gusain, K. Gupta, P. Joshi, O.P. Khatri, Adsorptive removal and photocatalytic degradation of organic pollutantsusing metal oxides and their composites: a comprehensive review, Adv. Colloid Interface Sci. 272 (2019), 102009.

[23] P. Yadav, P.K. Surolia, D. Vaya, Synthesis and application of copper ferrite-graphene oxide nanocomposite photocatalyst for the degradation of malachite green, Mater. Today Proc. 43 (2021) 2949–2953.

[24] M. Verma, M. Mitan, H. Kim, D. Vaya, Efficient photocatalytic degradation of Malachite green dye using facilely synthesized cobalt oxide nanomaterials using citric acid and oleic acid, J. Phys. Chem. Solids 155 (2021), 110125, https://doi.org/10.1016/j.jpcs.2021.110125.

[25] V. Nogueira, I. Lopes, T. Rocha-Santos, F. Gonçalves, R. Pereira, Treatment of real industrial wastewaters through nano-TiO_2 and nano-Fe_2O_3 photocatalysis: case study of mining and kraft pulp mill effluents, Environ. Technol. 39 (2017) 1586–1596, https://doi.org/10.1080/09593330.2017.1334093.

[26] S. Chakrabarti, B.K. Dutta, R. Apak, Active manganese oxide: a novel adsorbent for treatment of wastewater containing azo dye, Water Sci. Technol. 60 (2009) 3017–3024, https://doi.org/10.2166/wst.2009.758.

[27] R. Zhai, Y. Wan, L. Liu, X. Zhang, W. Wang, J. Liu, B. Zhang, Hierarchical MnO_2 nanostructures: synthesis and their application in water treatment, Water Sci. Technol. 65 (2012) 1054–1059, https://doi.org/10.2166/wst.2012.925.

[28] M. Verma, R. Chandra, V.K. Gupta, Decontamination of 2-chloro ethyl ethyl sulphide and dimethyl methyl phosphonate from aqueous solutions using manganese oxide nanostructures, J. Mol. Liq. 215 (2016) 285–292, https://doi.org/10.1016/j.molliq.2015.12.039.

[29] T. Chhabra, A. Kumar, A. Bahuguna, V. Krishnan, Reduced graphene oxide supported MnO_2 nanorods as recyclable and efficient adsorptive photocatalysts for pollutants removal, Vacuum 160 (2019) 333–346, https://doi.org/10.1016/j.vacuum.2018.11.053.
[30] H. Saroyan, G.Z. Kyzas, E.A. Deliyanni, Effective dye degradation by graphene oxide supported manganese oxide, Processes 7 (2019) 11–13, https://doi.org/10.3390/pr7010040.
[31] J. Wang, J. Zhang, L. Han, J. Wang, L. Zhud, H. Zeng, Graphene-based materials for adsorptive removal of pollutants from water and underlying interaction mechanism, Adv. Colloid Interface Sci. 289 (2021), 102360, https://doi.org/10.1016/j.cis.2021.102360.
[32] M. Verma, A. Kumar, K.P. Singh, R. Kumar, V. Kumar, C.M. Srivastava, V. Rawat, G. Rao, S. Kumari, P. Sharma, H. Kim, Graphene oxide-manganese ferrite (GO-$MnFe_2O_4$) nanocomposite: One-pot hydrothermal synthesis and its use for adsorptive removal of Pb^{2+} ions from aqueous medium, J. Mol. Liq. 315 (2020), 113769, https://doi.org/10.1016/j.molliq.2020.113769.
[33] M. Verma, I. Tyagi, R. Chandra, V.K. Gupta, Adsorptive removal of Pb (II) ions from aqueous solution using CuO nanoparticles synthesized by sputtering method, J. Mol. Liq. 225 (2017) 936–944, https://doi.org/10.1016/j.molliq.2016.04.045.
[34] H.L. Xu, W. De Zhang, Graphene oxide–MnO_2 nanocomposite-modified glassy carbon electrode as an efficient sensor for H_2O_2, Chinese, Chem. Lett. 28 (2017) 143–148, https://doi.org/10.1016/j.cclet.2016.10.008.
[35] C. Te Hsieh, H. Teng, W.Y. Chen, Y.S. Cheng, Synthesis, characterization, and electrochemical capacitance of amino-functionalized carbon nanotube/carbon paper electrodes, Carbon N.Y. 48 (2010) 4219–4229, https://doi.org/10.1016/j.carbon.2010.07.021.
[36] J. Zhong, F. Yi, Y. Huang, Preparation of 3d reduced graphene oxide/MnO_2 nanocomposites through a vacuum-impregnation method and their electrochemical capacitive behavior, Chemelectrochem 4 (2017) 1088–1094, https://doi.org/10.1002/celc.201600836.
[37] L. Ma, X. Shen, Z. Ji, G. Zhu, H. Zhou, Ag nanoparticles decorated MnO_2/reduced graphene oxide as advanced electrode materials for supercapacitors, Chem. Eng. J. 252 (2014) 95–103, https://doi.org/10.1016/j.cej.2014.04.093.
[38] J. Lei, X. Lu, W. Wang, X. Bian, Y. Xue, C. Wang, L. Li, Fabrication of MnO_2/graphene oxide composite nanosheets and their application in hydrazine detection, RSC Adv. 2 (2012) 2541–2544, https://doi.org/10.1039/C2RA01065H.
[39] C. Tsang, J. Kim, A. Manthiram, Synthesis of manganese oxides by reduction of $KMnO_4$ with KBH_4 in aqueous solutions, J. Solid State Chem. 137 (1998) 28–32, https://doi.org/10.1006/jssc.1997.7656.
[40] J. Chen, J. Zhu, N. Wang, J. Feng, W. Yan, Hydrophilic polythiophene/SiO_2 composite for adsorption engineering: green synthesis in aqueous medium and its synergistic and specific adsorption for heavy metals from wastewater, Chem. Eng. J. 360 (2019) 1486–1497, https://doi.org/10.1016/j.cej.2018.10.228.
[41] K.K. Jaiswal, V. Kumar, M.S. Vlaskin, M. Nanda, M. Verma, W. Ahmad, H. Kim, Hydropyrolysis of freshwater macroalgal bloom for bio-oil and biochar production: kinetics and isotherm for removal of multiple heavy metals, Environ. Technol. Innov. 22 (2021), 101440, https://doi.org/10.1016/j.eti.2021.101440.
[42] K.K. Jaiswal, V. Kumar, R. Verma, M. Verma, A. Kumar, M.S. Vlaskin, M. Nanda, H. Kim, Graphitic bio-char and bio-oil synthesis via hydrothermal carbonization-co-liquefaction of microalgae biomass (oiled/de-oiled) and multiple heavy metals remediations, J. Hazard. Mater. 409 (2021), 124987, https://doi.org/10.1016/j.jhazmat.2020.124987.
[43] W. Yang, M. Cheng, Y. Han, X. Luo, C. Li, W. Tang, T. Yue, Z. Li, Heavy metal ions' poisoning behavior-inspired etched UiO-66/CTS aerogel for Pb(II) and Cd(II) removal from aqueous and apple juice, J. Hazard. Mater. 401 (2021), 123318, https://doi.org/10.1016/j.jhazmat.2020.123318.
[44] M. Hong, Y. Wang, R. Wang, Y. Sun, R. Yang, L. Qu, Z. Li, Poly(sodium styrene sulfonate) functionalized graphene as a highly efficient adsorbent for cationic dye removal with a green regeneration strategy, J. Phys. Chem. Solids 152 (2021), 109973, https://doi.org/10.1016/j.jpcs.2021.109973.
[45] Y. Tang, T. Lin, S. Ai, Y. Li, R. Zhou, Y. Peng, Super and selective adsorption of cationic dyes using carboxylate-modified lignosulfonate by environmentally friendly solvent-free esterification, Int. J. Biol. Macromol. 159 (2020) 98–107, https://doi.org/10.1016/j.ijbiomac.2020.05.037.
[46] J.O. Amode, J.H. Santos, Z. Md Alam, A.H. Mirza, C.C. Mei, Adsorption of methylene blue from aqueous solution using untreated and treated (Metroxylon spp.) waste adsorbent: equilibrium and kinetics studies, Int. J. Ind. Chem. 7 (2016) 333–345, https://doi.org/10.1007/s40090-016-0085-9.
[47] H. Gao, Z. Song, W. Zhang, X. Yang, X. Wang, D. Wang, Synthesis of highly effective absorbents with waste quenching blast furnace slag to remove Methyl Orange from aqueous solution, J. Environ. Sci. 53 (2017) 68–77, https://doi.org/10.1016/j.jes.2016.05.014.
[48] S.S. Shah, T. Sharma, B.A. Dar, R.K. Bamezai, Adsorptive removal of methyl orange dye from aqueous solution using populous leaves: insights from kinetics, thermodynamics and computational studies, Environ. Chem. Ecotoxicol. 3 (2021) 172–181, https://doi.org/10.1016/j.enceco.2021.05.002.
[49] Z. Wang, Y. Ma, H. He, C. Pei, P. He, A novel reusable nanocomposite: FeOOH/CBC and its adsorptive property for methyl orange, Appl. Surf. Sci. 332 (2015) 456–462, https://doi.org/10.1016/j.apsusc.2015.01.160.
[50] D. Pathania, S. Sharma, P. Singh, Removal of methylene blue by adsorption onto activated carbon developed from Ficus carica bast, Arab. J. Chem. 10 (2017) S1445–S1451, https://doi.org/10.1016/j.arabjc.2013.04.021.
[51] M. Tanhaei, A.R. Mahjoub, V. Safarifard, Sonochemical synthesis of amide-functionalized metal-organic framework/graphene oxide nanocomposite for the adsorption of methylene blue from aqueous solution, Ultrason. Sonochem. 41 (2018) 189–195, https://doi.org/10.1016/j.ultsonch.2017.09.030.
[52] S. Tahazadeh, H. Karimi, T. Mohammadi, H.B.M. Emrooz, M.A. Tofighy, Fabrication of biodegradable cellulose acetate/MOF-derived porous carbon nanocomposite adsorbent for methylene blue removal from aqueous solutions, J. Solid State Chem. 299 (2021), 122180, https://doi.org/10.1016/j.jssc.2021.122180.